


RESEARCH ARTICLE

Open Access



The novel tRNA-derived fragment, tiRNA-Met, inhibits the malignant progression of triple-negative breast cancer by regulating RANBP3L via a targeted interaction with SNRPA

Jingjing Lu^{1,3†}, Yangbai Sun^{4†}, Xiufen Zhang^{1,7}, Bujie Xu¹, Ping Zhu⁵, Linzi Zeng¹, Xue Wang⁶, Wei Zhu^{2*} and Ping Zhou^{1*} 

[†]Jingjing Lu and Yangbai Sun have contributed equally to this work.

*Correspondence: zhu.wei1@zs-hospital.sh.cn; zping@shmu.edu.cn

¹ Department of Physiology and Pathophysiology, School of Basic Medical Sciences, Fudan University, No.138 Yixueyuan Road, Shanghai 200032, China

² Department of General Surgery, Zhongshan Hospital, Fudan University, No.111 Yixueyuan Road, Shanghai 200032, China

³ Clinical Medical Research Center, Affiliated Hospital of Nantong University, Nantong 226019, Jiangsu, China

⁴ Department of Musculoskeletal Oncology, Fudan University Shanghai Cancer Center, Fudan University, Shanghai 200032, China

⁵ Department of Pathology, Fudan University Shanghai Cancer Center, Shanghai Medical College, Fudan University, Shanghai 200032, China

⁶ Department of Pathology, Ruijin Hospital, Shanghai Jiao Tong University School of Medicine, Shanghai 200032, China

⁷ Oncology Institute, Affiliated Hospital of Jiangnan University, Wuxi 214062, Jiangsu, China

Abstract

Background: tRNA-derived fragments (tRFs) have emerged as significant noncoding RNAs in cancer biology; however, their roles and mechanisms in triple-negative breast cancer (TNBC) remain inadequately characterized.

Methods: tRF and tiRNA sequencing, real-time quantitative polymerase chain reaction (RT-qPCR), fluorescence in situ hybridization (FISH), and subcellular fractionation were used to explore the expression and characteristic of tiRNA-Met in TNBC. The biological functions of tiRNA-Met were assessed using CCK-8 assays, colony formation assays, and Transwell assays in vitro, alongside mouse xenograft models in vivo. RNA pull-down, mass spectrum, RNA immunoprecipitation (RIP), western blot, ubiquitination assays, RNA sequencing, actinomycin D assays, immunofluorescence, immunohistochemical staining, and rescue experiments were performed to explore the regulatory mechanisms of tiRNA-Met in TNBC.

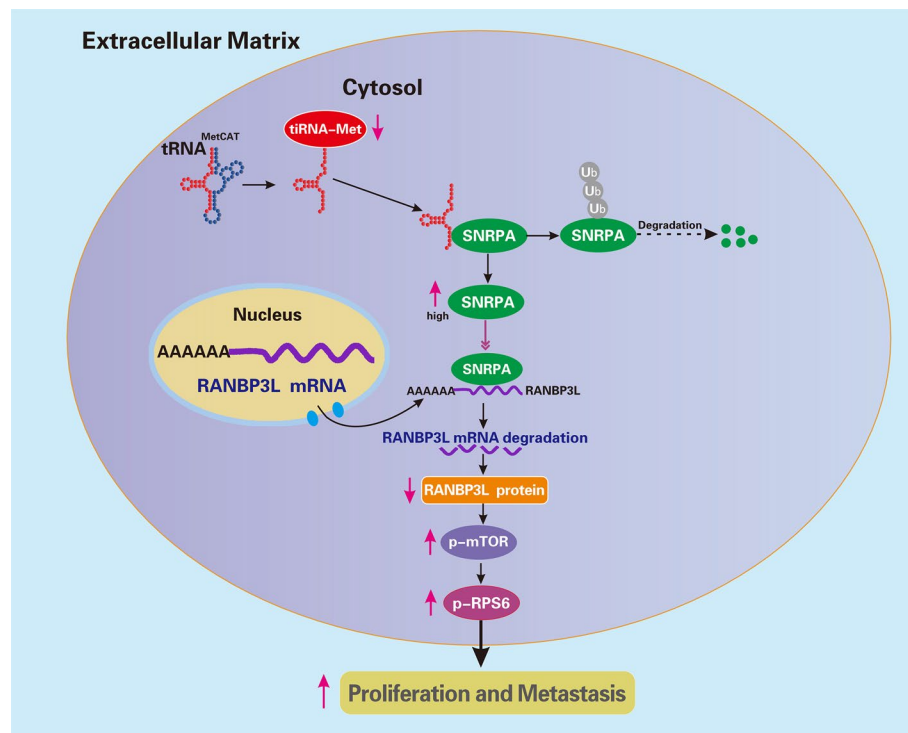
Results: tiRNA-Met was an uncharacterized tRF that originated from mitochondrial tRNA^{Met-CAT} and was primarily localized in the cytoplasm. Its expression was significantly downregulated in TNBC tumor tissues compared with adjacent normal tissues. Overexpression of tiRNA-Met markedly inhibited the proliferation, migration, and invasion of TNBC cells; whereas, its reduced expression elicited opposite effects. In addition, tiRNA-Met overexpression suppressed TNBC cell growth in vivo. Mechanistically, tiRNA-Met directly interacted with the RNA recognition motif 2 (RRM2) domain of small nuclear ribonucleoprotein A (SNRPA), promoting SNRPA protein degradation via the ubiquitin/proteasome pathway. This interaction enhanced the stability of Ran-binding protein 3-like (*RANBP3L*) mRNA, resulting in increased *RANBP3L* expression and subsequent inhibition of the mTORC1/RPS6 signaling pathway.

Conclusions: Our study identified tiRNA-Met as a novel anti-oncogenic tRF and elucidated its mechanism for inhibiting the malignancy of TNBC. tiRNA-Met directly bound to SNRPA, promoting its degradation and stabilizing *RANBP3L* mRNA, ultimately leading to the inhibition of the mTORC1 signaling pathway. These findings position tiRNA-Met as a promising candidate for diagnostic and therapeutic applications in TNBC.



Keywords: tRNA-derived fragment, tiRNA-Met, SNRPA, RANBP3L, Triple-negative breast cancer

Graphical Abstract



Background

Breast cancer is currently the most commonly diagnosed malignant tumor worldwide, with the highest incidence and mortality rates among all cancer types affecting women [1]. Triple-negative breast cancer (TNBC), representing approximately 15–20% of all types of breast cancer, is one of the most aggressive subtypes. TNBC is characterized by early onset, high invasiveness, propensity for metastasis, elevated recurrence rates, poor clinical prognosis, and low survival rates. Due to the absence of estrogen receptors (ER), progesterone receptors (PR), and human epidermal growth factor receptor 2 (HER2) expression, traditional therapies such as endocrine therapy and HER2-targeted therapy are ineffective. Chemotherapy remains the primary systemic treatment [2, 3]. With the advancement of molecular subtyping in TNBC, targeted therapies have begun to emerge as potential treatment options. Key targets for these therapies include poly (ADP-ribose) polymerase (PARP), androgen receptor (AR), epidermal growth factor receptor (EGFR), and vascular endothelial growth factor (VEGF). However, the therapeutic efficacy of many targeted agents in TNBC has yet to meet clinical expectations [4–6]. Therefore,

there is an urgent need to identify effective biomarkers and therapeutic targets for the treatment of TNBC.

The rapid advancement of high-throughput sequencing technology has led to the discovery of additional noncoding RNAs (ncRNAs) and their diverse functions. To date, the biological roles and pathological significance of long noncoding RNAs (lncRNAs), circular RNAs (circRNAs), and microRNAs (miRNAs) have been extensively studied [7, 8]. Recent research has highlighted the importance of tRNA-derived fragments (tRFs)—a class of small noncoding RNAs (sncRNAs)—in tumorigenesis and progression, positioning tRFs as potential molecular markers and novel therapeutic targets for cancer diagnosis and treatment [9–11].

tRFs are sncRNAs ranging from approximately 14 to 50 nucleotides (nt) in length, generated through the cleavage of mature or precursor tRNAs at specific sites. On the basis of the regions from which they are derived, tRFs can be classified into three categories: (1) tRF-1s, which originate from the 3' end of pre-tRNAs; (2) tRF-3s, tRF-5s, and i-tRFs (also referred to as tRF-2s); and (3) tRNA-halves (tiRNAs). tRF-3s result from cleavage at the TΨC loop of tRNAs and are mainly divided into two subtypes: tRF-3a (18 nt) and tRF-3b (22 nt). tRF-5s are formed by cleavage within the stem region between the D loop and anticodon, further classified into three subtypes based on length: tRF-5a (14–16 nt), tRF-5b (22–24 nt), and tRF-5c (28–30 nt). Lastly, i-tRFs are derived from mature tRNA-Glu, tRNAAsp, tRNA^{Gly}, and tRNA^{Tyr}, containing only the anticodon loop and stem of the tRNA. tRNA-halves (tiRNAs) are produced by the specific cleavage of mature tRNAs at the anticodon loop, primarily by angiogenin, with lengths ranging from approximately 29 to 50 nt. tiRNAs can be further categorized into tiRNA-3s and tiRNA-5s [9, 10, 12, 13].

Accumulating evidence has elucidated the connection between tRFs and tumor progression. For instance, tRF-21, regulated by inflammation, bound to heterogeneous nuclear ribonucleoprotein L (HNRNPL), inhibiting its phosphorylation and diminishing its capacity to associate with DDX17, ultimately suppresses malignant transformation in pancreatic ductal adenocarcinoma [14]. The pan-cancer tRNA-derived fragment CAT1 associated with RBPM5 to enhance the stability of *NOTCH2* mRNA, thereby facilitating the proliferation and metastasis of lung cancer cells [15]. In breast cancer, 5'-tiRNA^{Val} directly bound to the 3' untranslated region (UTR) of *FZD3*, resulting in decreased *FZD3* expression and subsequent inhibition of tumor formation and metastasis via the *FZD3*/Wnt/ β -catenin signaling pathway [16]. In thyroid cancer, tiRNA-Gly targeted the U2AF homology motif (UHM) domain of splicing factor RBM17 to promote its nuclear translocation and prevent degradation, thereby inducing alternative splicing of *MAP4K4* and facilitating tumor progression [17]. The 3' tRNA-derived fragment tRF-Val enhanced tumor progression by binding to *EEF1A1* and mediating p53 ubiquitination in gastric cancer [18]. A novel tRF, AS-tDR-007333, increased *MED29* expression by binding to *HSPB1* and inducing H3K4me1 and H3K27ac modifications in the *MED29* promoter region, thereby promoting malignant progression in non-small cell lung cancer [19]. In colorectal cancer, tRF-3022b modulated tumor growth and M2 macrophage polarization by interacting with *LGALS1* and *MIF* [20].

Herein, we report that tiRNA-Met, a novel human-specific tRF derived from mitochondrial tRNA^{Met-CAT}, was significantly downregulated in TNBC tissues and inhibited

tumor progression both in vitro and in vivo. The interaction between tiRNA-Met and the RNA-binding protein SNRPA promoted SNRPA ubiquitination and degradation, leading to the stabilization of *RANBP3L* mRNA and inhibition of the mTORC1 signaling pathway. This study might provide new insights into the mechanisms underlying TNBC progression and highlight the potential of tiRNA-Met as a novel diagnostic and therapeutic target for TNBC treatment.

Methods

Clinical samples

All TNBC tissues and adjacent normal tissues were obtained from patients who underwent surgical resection at the Department of Breast Surgery, Zhongshan Hospital, Fudan University, Shanghai, China, and the Department of Pathology, Ruijin Hospital, affiliated with Shanghai Jiao Tong University, Shanghai, China. All participants provided written informed consent for the study. This research was approved by the Ethics Committee of the School of Basic Medical Sciences, Fudan University (approval no. 2021-C025).

Cell lines and cell culture

Immortalized human TNBC cell lines MDA-MB-231 (cat. no. SCSP-5043) and BT-549 (cat. no. TCHu 93), as well as human mammary epithelial cells MCF 10A (cat. no. SCSP-575), were sourced from the Type Culture Collection of the Chinese Academy of Sciences (Shanghai, China). MDA-MB-231 cells were cultured in Leibovitz's L-15 medium (Gibco, USA) supplemented with 10% fetal bovine serum (FBS; Gibco, USA) at 37 °C in a humidified incubator without CO₂. BT-549 cells were maintained in RPMI 1640 medium (Gibco, USA) with 10% FBS at 37 °C in a humidified incubator containing 5% CO₂. All culture media were further supplemented with Penicillin–Streptomycin Liquid (penicillin, 100 units/ml; streptomycin, 100 µg/ml; NCM Biotech, Jiangsu, China). MCF 10A cells were cultured in complete culture medium (cat. no. SCSP-660S) obtained from the Type Culture Collection of the Chinese Academy of Sciences (Shanghai, China), also at 37 °C in a humidified incubator with 5% CO₂. All cell lines were verified to be free of mycoplasma contamination.

Transient transfection and lentivirus infection

The tiRNA-Met overexpression model and inhibition model, along with corresponding controls, were established by transfecting cells with tiRNA-Met mimics, inhibitors, and negative control (NC) oligonucleotides. These constructs were designed and synthesized by RiboBio (Guangzhou, China). In addition, small interfering RNAs (siRNAs) targeting *RANBP3L* (si-RANBP3L) and *SNRPA* (si-SNRPA), as well as a negative control siRNA (si-NC), were designed and synthesized by GenePharma (Shanghai, China). Plasmids for Flag-fused RANBP3L, Flag-fused wild-type (WT) SNRPA, and truncated SNRPA were purchased from Genechem (Shanghai, China). Transfections were performed using Lipofectamine 3000 reagent (Invitrogen, CA, USA) according to the manufacturer's instructions, with final concentrations of 50 nM for mimics and siRNAs, 100 nM for inhibitors, and 1 µg/ml for plasmids. The lentiviral vector for tiRNA-Met overexpression and the control lentiviral vector were purchased from GenePharma (Shanghai, China).

Cells were infected and selected with 1 µg/ml puromycin (Beyotime, Shanghai, China). All interfering sequences used in this study are listed in Supplementary Table S1.

RT-qPCR

Total RNA was extracted from TNBC tissue samples and cell lines using TRIzol® reagent (Invitrogen, CA, USA). Reverse transcription for tiRNA-Met was performed using an miRNA 1st Strand cDNA Synthesis Kit (MR101-01, Vazyme, Nanjing, China), while mRNA reverse transcription was conducted with a HiScript® III 1st Strand cDNA Synthesis Kit (+gDNA wiper) (R312-01, Vazyme, Nanjing, China), following the manufacturer's protocols. The cDNA amplification was carried out using the Taq Pro Universal SYBR qPCR Master Mix (Q712-02, Vazyme, Nanjing, China) with an ABI QuantStudio 5 detection system (Applied Biosystems, TX, USA). The relative levels of mRNAs and tiRNA-Met were normalized to *GAPDH* mRNA levels and U6 small RNA levels, respectively. Each experiment included three biological replicates, and relative expression levels were calculated using the $2^{-\Delta\Delta C_t}$ method. Primer sequences are provided in Supplementary Table S2.

Subcellular fractionation

Cytosolic and nuclear components from MDA-MB-231, BT-549, and MCF 10A cells were prepared using the PARIS™ Kit Protein and RNA Isolation System (AM1921, Thermo Fisher, MA, USA) according to the manufacturer's instructions. The RNA harvested from both the cytosolic and nuclear fractions was subsequently subjected to RT-qPCR.

Western blot

Total proteins were extracted from cells using RIPA lysis buffer (Beyotime, Shanghai, China). Protein concentrations were determined using a BCA kit (Vazyme, Nanjing, China). Equal amounts of protein were loaded onto SDS-PAGE gels (EpiZyme, Shanghai, China) and subsequently transferred to PVDF membranes (Millipore, MA, USA). Membranes were blocked for 2 h at room temperature with 5% nonfat milk. Each membrane was then incubated overnight at 4 °C with primary antibodies. Following the primary antibody incubation, membranes were washed three times with Tris-buffered saline with Tween 20 (TBS-T) and then incubated with horseradish peroxidase (HRP)-conjugated secondary antibodies diluted in 5% bovine serum albumin (BSA) for 2 h at room temperature. Chemiluminescent detection reagents (Vazyme, Nanjing, China) were applied to visualize protein bands using a ChemiDoc MP system (Bio-Rad, CA, USA), and ImageJ software was used for image analysis. The following antibodies were utilized in this study: anti-RANBP3L (no. R86197, Sigma), anti-SNRPA (no. 10,212-1-AP, Proteintech), anti-Flag (no. 14793S, Cell Signaling Technology), anti-ubiquitin (no. 10,201-2-AP, Proteintech), anti-RPS6 (no. TN25622, Abmart), anti-mTOR (no. T55306, Abmart), anti-phospho-RPS6 (no. PA4217, Abmart), anti-phospho-mTOR (no. T56571, Abmart), anti-β-actin (no. HRP-66009, Proteintech), anti-rabbit IgG-HRP (no. A0208, Beyotime), and anti-mouse IgG-HRP (no. A0216, Beyotime).

RNA sequencing

RNA sequencing was performed to identify the target genes regulated by tiRNA-Met. MDA-MB-231 cells were transfected with either tiRNA-Met mimics or NC for 48 h, after which, RNA was extracted from the treated cells using TRIzol[®] reagent. The RNA samples were then sent to RiboBio (Guangzhou, China) for comprehensive RNA sequencing analysis.

RNA pull-down assay and mass spectrometry

Biotin-labeled tiRNA-Met sense and antisense sequences were obtained from Genescript (Nanjing, China). RNA pull-down assays were conducted using a Pierce[™] Magnetic RNA-Protein Pull-Down Kit (no. 20,164, Thermo Fisher, MA, USA) according to the manufacturer's instructions. The resulting RNA-protein complexes were boiled in 20 µl of 1× loading buffer, subjected to 10% SDS-PAGE (EpiZyme, Shanghai, China), and silver stained (Beyotime, Shanghai, China). Protein bands exhibiting significant differences were excised and sent to Shanghai Applied Protein Technology (Shanghai, China) for mass spectrometry analysis. Eluate containing proteins associated with tiRNA-Met from RNA pull-down was firstly digested into peptides. Subsequently, liquid chromatography-tandem mass spectrometry (LC-MS/MS) analysis was performed on a timsTOF Pro mass spectrometer (Bruker) over a duration of 30 min. Solvent A consisted of 0.1% formic acid in water, while Solvent B was composed of 0.1% formic acid in acetonitrile. The peptides were loaded in 95% Solvent A and separated using a Thermo Scientific EASY column (15 cm, ID 150 µm, 3 µm, C18) with a 30-min gradient at a flow rate of 300 nl/min: 5% to 35% B over 18 min; 35% to 80% B over 2 min; and hold at 80% B for 10 min. The data were analyzed using MaxQuant software (version 1.6.14).

RIP assay

RIP assays were conducted using a Magna RNA-binding protein immunoprecipitation kit (no. 17-704; Millipore, MA, USA) following the manufacturer's instructions. MDA-MB-231 and BT-549 cells (1×10^7) were lysed in 1 ml of RIP lysis buffer supplemented with RNase inhibitors (Beyotime, Shanghai, China). Magnetic beads (Bio-Rad, CA, USA) were subsequently incubated with anti-SNRPA (no. 10,212-1-AP; Proteintech) or anti-IgG (no. A7016; Beyotime) antibodies. The resulting complexes were then incubated with total RNA lysates. The RNA bound to the complexes was extracted and purified, and the presence of specific RNA sequences was verified by RT-qPCR.

Immunoprecipitation

MDA-MB-231 cells, transfected with either NC or tiRNA-Met mimics, were lysed using a lysis buffer containing protease inhibitors (Roche, P8340, Shanghai, China). The lysates were centrifuged to remove cellular debris, and the resulting supernatants were collected. Thirty microliters of Protein A/G magnetic beads (Bio-Rad, CA, USA) were washed and resuspended in an appropriate buffer. Then, 3 µg of anti-SNRPA antibody (no. 10,212-1-AP; Proteintech) or anti-IgG antibody (no. A7016; Beyotime) was added to the bead suspension, which was incubated for 4 h at 4 °C to allow the antibodies to bind to the beads. The lysate supernatants were then added to the antibody-bound beads and incubated overnight at 4 °C with gentle rotation to facilitate the formation of

antibody–protein complexes. The antibody–protein complexes were subsequently isolated using a magnetic stand. Finally, the proteins were extracted and subjected to qualitative western blot analysis.

Cell proliferation and colony formation assays

MDA-MB-231 and BT-549 cells were transfected with 50 nM tiRNA-Met mimics, 100 nM inhibitors, or NC and incubated for 48 h. Following incubation, the cells were dispersed into 96-well plates at a density of 2×10^3 cells per well and cultured for 5 days at 37 °C. Cell viability was periodically assessed using a Cell Counting Kit-8 (Yeasen, Shanghai, China). For colony formation assays, cells were seeded in six-well plates at a density of 500 cells in 2 ml of medium and maintained for 7–10 d, during which the medium was exchanged daily. Colonies were subsequently fixed with 4% paraformaldehyde for 15 min and stained with crystal violet (Beyotime, Shanghai, China) for 5 min; they were then counted and imaged.

Transwell assay

For the migration assay, a standard Transwell chamber (no. 353,097; BD, NJ, USA) was employed, while for the invasion assay, a Transwell chamber precoated with Matrigel was used (no. 356,234; BD, NJ, USA). Specifically, the upper chamber was seeded with 200 μ l of cells (3×10^4 cells for the migration assay and 5×10^4 cells for the invasion assay) in FBS-free medium. The lower chamber contained medium supplemented with 20% FBS to stimulate migration. The complete Transwell system was incubated at 37 °C for 24 h. Following incubation, any residual cells in the upper chamber were carefully removed, and the cells that migrated through the membrane were stained with 0.5% crystal violet staining solution (Beyotime, Shanghai, China) for 5 min. Stained cells were then examined and imaged under a microscope (Olympus, Tokyo, Japan).

Actinomycin D assays

MDA-MB-231 and BT-549 cells were separately transfected with either NC or si-SNRPA. After a 24 h transfection period, actinomycin D (10 μ g/ml; MCE, NJ, USA) was administered to the cells, and samples were systematically collected every 2 h. RNA was extracted from the samples and subsequently subjected to RT-qPCR to assess the mRNA stability of *RANBP3L*.

RNA fluorescence in situ hybridization

The tiRNA-Met probe and Fluorescent In Situ Hybridization Kit were obtained from GenePharma (Shanghai, China). Procedures were carried out according to the manufacturer's instructions provided in the manual.

Immunofluorescence

MDA-MB-231 and BT-549 cells (2×10^3 per well) were seeded in a cell migration apparatus and allowed to settle undisturbed overnight. The cells were then fixed with 4% paraformaldehyde for 15 min and treated with 0.1% Triton X-100 in phosphate-buffered saline (PBS) for 10 min. Following this, the cells were blocked with 5% BSA at 37 °C for 30 min and incubated overnight at 4 °C with a primary anti-RANBP3L antibody (no.

17,875–1-AP; Proteintech). Then, the cells were stained with Cy3-conjugated secondary antibody (no. A0516, Beyotime). After thorough washing three times with PBS, the cells were stained with DAPI (no. C1002, Beyotime) for 5 min. Images were captured using a fluorescence microscope (Olympus, Tokyo, Japan).

Immunohistochemistry

Paraffin-embedded tissue samples were deparaffinized by incubating at 65 °C for 20 min, followed by clearing with xylene and rehydration through a series of graded alcohol solutions. Antigen retrieval was performed by heating the slides in saline sodium citrate buffer at 95–100 °C. After cooling and washing twice with PBS, the slides were incubated overnight at 4 °C with primary antibodies against Ki-67 (no. 27,309–1-AP; Proteintech), RANBP3L (no. R86197; Sigma), and SNRPA (no. 10,212–1-AP; Proteintech), diluted in blocking solution. This was followed by a 1 h incubation at room temperature with a horseradish peroxidase-conjugated secondary antibody. The slides were subsequently developed using 3,3'-diaminobenzidine, counterstained with hematoxylin, and dehydrated through graded ethanol solutions. Staining density was observed under a fluorescence microscope (Olympus, Tokyo, Japan). Ki67 was assessed by determining the percentage of positively stained cells. The labeling intensity for RANBP3L and SNRPA was categorized as follows: negative (0), weak (1), moderate (2), and strong (3). The extent of staining, measured by the percentage of positively stained cells, was scored as follows: 1 ($\leq 25\%$), 2 (26–50%), 3 (51–75%), and 4 ($> 75\%$) [14].

In vivo mouse model

To better understand the functional roles of tiRNA-Met in a live biological context, tumor xenografts were generated in 4-week-old female BALB/c nude mice. The mice were randomly assigned to each group ($n=6$ mice per group). MDA-MB-231 cells stably transfected with either LV-tiRNA-Met or control LV-ctrl (5×10^6 , 150 μ l; GenePharma, Shanghai, China) were subcutaneously injected into the mammary fat pads of the nude mice. Tumor dimensions were monitored weekly. After 4 weeks, the mice were humanely euthanized, and the tumors were meticulously excised and prepared for immunohistochemical examination. All animal experimental procedures were approved by the Ethics Committee for Laboratory Animals of the School of Basic Medical Sciences, Fudan University (approval no. 20210302–001).

Data sources and gene expression analysis

To investigate the expression of RANBP3L and SNRPA in pan-cancer and normal samples, we accessed The Cancer Genome Atlas (TCGA) and GTEx data through the University of California, Santa Cruz (UCSC) Xena website (<https://xena.ucsc.edu/>). Data analysis was conducted using R software (version 4.3.0) with the “ggplot2” and “ggpubr” packages.

The BRCA dataset from the TCGA database was obtained using the TCGAbiolinks package in R (version 4.3.0). The downloaded dataset was filtered on the basis of subtype information, and the expression levels of RANBP3L and SNRPA across different BRCA subtypes were analyzed using the aforementioned methods.

UALCAN database

UALCAN (<http://ualcan.path.uab.edu/>) is an extensive, user-friendly platform for exploring cancer OMICS data.

Correlation analysis

Gene expression data for RANBP3L and SNRPA were obtained from the TCGA database via the UCSC Xena website. The correlation between RANBP3L and SNRPA expression in TNBC samples was analyzed using R software (version 4.3.0) with the “dplyr” and “tibble” packages.

Kaplan–Meier analysis

A Kaplan–Meier plot of overall survival (OS) was generated with Kaplan–Meier Plotter (<http://kmplot.com/analysis/>).

Statistical analysis

All statistical analyses were performed using SPSS statistical software (version 22) and GraphPad Prism (version 8.0). Data from at least three independent experiments were presented as means \pm standard deviation (SD). Comparisons of tiRNA-Met expression between paired specimens were analyzed using the Wilcoxon matched-pairs signed-rank test. A two-way analysis of variance (ANOVA) was performed to analyze the results of the CCK-8 assays. The correlation between RANBP3L and SNRPA was assessed using Pearson's correlation coefficient. A *P*-value of less than 0.05 was considered statistically significant.

Results

tiRNA-Met was significantly downregulated in TNBC tissues and inhibited TNBC tumorigenesis

In our previous research, we discovered the expression profiles of tRFs in TNBC by comparing samples from three pairs of TNBC tissues and their adjacent normal tissues. This analysis identified 306 tRFs: 216 were coexpressed in both tissue types, 56 were specifically found in adjacent normal tissues, and 34 were exclusive to tumor tissues. Using the R package edgeR with fold change and *P*-value cutoffs of 1.5 and 0.05, a total of 42 upregulated and 19 downregulated tRFs were identified in TNBC. An expanded clinical sample size confirmed the expression patterns of four tRFs, consistent with sequencing results. Notably, tRF^{His-GTG-006} and tRF^{Lys-CTT-010} were significantly increased in tumor tissues, while tiRNA-Met (tRF^{Met-CAT-012}) was downregulated; no significant difference was observed for tRF^{Ser-TGA-001} [21]. Among these tRFs, tiRNA-Met is a novel tiRNA originating from mitochondrial tRNA^{Met-CAT} and cleaved at positions 1 to 29 on the 5' end (Fig. 1A, B). We further analyzed the levels of tiRNA-Met in 77 pairs of TNBC tissues and adjacent normal tissues. The results indicated significantly lower levels of tiRNA-Met in tumor tissues (Fig. 1C). In addition, tiRNA-Met expression in MDA-MB-231 and BT-549 cells was markedly reduced compared with that in MCF 10A cells (Fig. 1D). Fluorescence in situ hybridization (FISH) and nuclear–cytoplasmic fractionation analyses revealed that tiRNA-Met

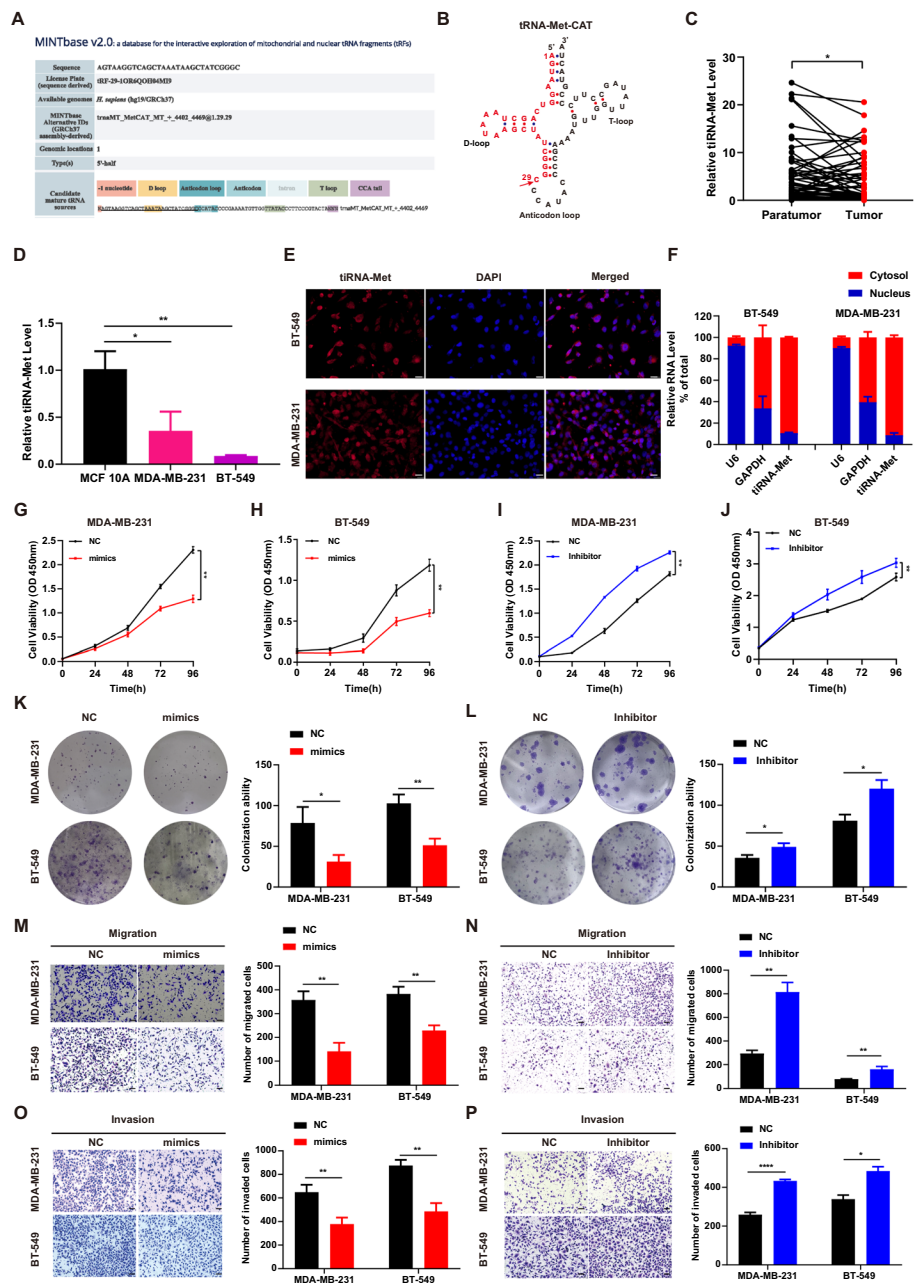


Fig. 1 Characterization of tiRNA-Met and its role in suppressing the malignant phenotypes of TNBC cells. **A** tiRNA-Met, derived from mitochondrial tRNA^{Met-CAT}, belongs to the tiRNA-5 fragment family. **B** Schematic representation and sequence of tiRNA-Met, which originates from mature tRNA^{Met-CAT}. **C** The expression of tiRNA-Met in TNBC tissues was significantly lower than that in paired adjacent normal tissues ($n = 77$). **D** Expression levels of tiRNA-Met in TNBC cell lines (MDA-MB-231 and BT-549) were lower than those in normal breast epithelial cells (MCF 10A). **E, F** Subcellular localization analysis via RNA FISH (**E**) and RT-qPCR (**F**) indicated that tiRNA-Met was predominantly localized in the cytoplasm of TNBC cells, with U6 and GAPDH serving as nuclear and cytoplasmic markers, respectively. Scale bars represent 50 μ m. **G–L** CCK-8 assays (**G–J**) and colony formation assays (**K, L**) demonstrated that overexpression of tiRNA-Met inhibited the proliferation rates of MDA-MB-231 and BT-549 cells, while knockdown of tiRNA-Met using an inhibitor promoted cell proliferation in both cell lines. **M–P** Transwell assays revealed that upregulation of tiRNA-Met decreased the number of migrated and invaded cells (**M, O**), whereas knockdown of tiRNA-Met resulted in increased migration and invasion (**N, P**). Scale bars represent 100 μ m. All data are presented as means \pm SD; * $P < 0.05$, ** $P < 0.01$, *** $P < 0.0001$

was predominantly localized in the cytoplasm (Fig. 1E, F; Supplementary Fig. S1). By modulating the expression of tiRNA-Met in cells—either through upregulation (Supplementary Fig. S2A, B) or downregulation (Supplementary Fig. S2C, D)—we observed its effects on cellular phenotypes. Overexpression of tiRNA-Met significantly inhibited cell proliferation (Fig. 1G, H, K), while suppression of tiRNA-Met expression had the opposite effect (Fig. 1I, J, L). Furthermore, increasing tiRNA-Met levels significantly reduced cell migration and invasion (Fig. 1M, O), whereas decreasing tiRNA-Met levels significantly enhanced these abilities (Fig. 1N, P). These findings suggested that tiRNA-Met may function as a tumor suppressor, inhibiting the malignant progression of TNBC.

tiRNA-Met directly interacted with SNRPA and enhanced the ubiquitin/proteasome-mediated degradation of SNRPA

To elucidate the mechanism by which tiRNA-Met exerted its biological functions in TNBC, we conducted RNA pull-down experiments followed by mass spectrometry analysis in TNBC cells (Fig. 2A, B). The results revealed that 67 and 35 proteins interacted with tiRNA-Met in MDA-MB-231 and BT-549 cells, respectively, while these proteins did not interact with the antisense RNA. Importantly, we focused on SNRPA for further investigation, as its binding to tiRNA-Met was consistently observed in both cell lines, and it is a common RNA-binding protein. The interaction between SNRPA and tiRNA-Met was further confirmed through western blot analysis of the RNA pull-down products (Fig. 2C). In addition, a RIP assay using an antibody against SNRPA demonstrated that tiRNA-Met specifically bound to endogenous SNRPA (Fig. 2D, E). We further conducted protein domain mapping assays using FLAG-tagged full-length and truncated SNRPA, revealing that the RRM2 domain (208–282 aa) of SNRPA is essential for their interaction (Fig. 2F).

Given the interaction between tiRNA-Met and SNRPA, we aimed to investigate the downstream molecular consequences of this association. Overexpression or knockdown of tiRNA-Met did not change *SNRPA* mRNA levels (Fig. 2G). However, overexpression significantly reduced SNRPA protein levels, while knockdown resulted in a marked increase in its protein expression (Fig. 2H). Following treatment with the protein synthesis inhibitor cycloheximide (Chx), transfection with tiRNA-Met decreased the half-life of the endogenous SNRPA protein in MDA-MB-231 cells (Fig. 2I). After treatment with the proteasome inhibitor MG132, SNRPA protein levels accumulated over time (Fig. 2J). These results suggested that tiRNA-Met enhanced the proteasome-dependent degradation of SNRPA in TNBC. In addition, overexpression of tiRNA-Met noticeably increased the levels of ubiquitinated SNRPA (Fig. 2K). Collectively, these results illustrated that tiRNA-Met reduced the stability of the SNRPA protein via a ubiquitin/proteasome-dependent degradation pathway.

SNRPA was elevated in TNBC tissues and attenuation of SNRPA rescued the effect of tiRNA-Met on TNBC cells

To further investigate the role of SNRPA, we conducted a bioinformatics analysis and found that SNRPA was upregulated in 21 different tumor types, including breast cancer (Supplementary Fig. S3A). The majority of TNBC are classified as the basal-like subtype

according to the PAM50 profile [22]. By utilizing PAM50, we classified the TCGA breast cancer dataset into distinct subtypes and found that SNRPA exhibited the highest expression levels specifically in the basal-like breast cancer subtype (Fig. 3A). More importantly, the analysis using the UALCAN database further confirmed that SNRPA had the highest expression levels in the TNBC subtype (Supplementary Fig. S3B). Moreover, SNRPA expression exhibited a negative correlation with OS in both breast cancer (Supplementary Fig. S3C) and patients with TNBC (Fig. 3B). Subsequently, we analyzed SNRPA expression in human TNBC tissue samples, confirming that SNRPA levels were significantly increased in tumor tissues compared with adjacent normal tissues (Fig. 3C). Immunohistochemistry further validated these findings, demonstrating a significant upregulation of SNRPA expression in human TNBC tissues relative to adjacent normal tissues (Fig. 3D). Consistent with this observation, the mRNA levels of *SNRPA* in MDA-MB-231 and BT-549 cells were higher than those in MCF 10A cells (Fig. 3E).

To further investigate whether tiRNA-Met inhibited the malignant progression of TNBC through its interaction with SNRPA, we conducted a “rescue” experiment by transfecting a tiRNA-Met inhibitor with or without SNRPA knockdown. The knockdown efficiency was confirmed by RT-qPCR (Supplementary Fig. S4A, B). Notably, the knockdown of SNRPA significantly enhanced the effects of tiRNA-Met on the proliferation (Fig. 3F, G), migration (Fig. 3H), and invasion (Fig. 3I) of MDA-MB-231 and BT-549 cells. In summary, we demonstrated that tiRNA-Met influenced the progression of malignancy in TNBC through its regulation of SNRPA expression.

tiRNA-Met upregulated the expression of RANBP3L via SNRPA

To further investigate the downstream target genes influenced by tiRNA-Met through its regulation of SNRPA, we performed RNA sequencing analysis in MDA-MB-231 cells overexpressing tiRNA-Met and in NC cells (Fig. 4A). The results revealed that tiRNA-Met overexpression led to the dysregulation of 779 genes, with 737 genes upregulated and 42 genes downregulated (Fig. 4B). Among these dysregulated genes, *RANBP3L* emerged as a candidate target for further exploration due to its significant changes in expression (Fig. 4C). We then confirmed the relationship between tiRNA-Met and *RANBP3L* by transfecting TNBC cells with tiRNA-Met mimics, resulting in a significant increase in *RANBP3L* expression (Fig. 4D). Conversely, suppression of tiRNA-Met led to a marked reduction in *RANBP3L* levels (Fig. 4E). Immunofluorescence assays further validated the enhanced expression of *RANBP3L* upon tiRNA-Met overexpression (Fig. 4F). To investigate the role of SNRPA in this regulatory pathway, we knocked down SNRPA in TNBC cells using si-SNRPA, which resulted in a notable increase in both mRNA and protein levels of *RANBP3L* (Fig. 4G, H). In addition, bioinformatics analysis revealed a negative correlation between the mRNA expression levels of the two genes in TNBC (Fig. 4I). Collectively, these findings suggested that SNRPA might play a crucial role in mediating the effects of tiRNA-Met on *RANBP3L* expression.

Given that SNRPA is an RNA-binding protein involved in alternative splicing and mRNA stability [23, 24], it would be intriguing to investigate whether SNRPA influences the alternative splicing of *RANBP3L* or affects its stability in interaction with tiRNA-Met. We conducted an alternative splicing analysis on the RNA sequencing results from the tiRNA-Met overexpression model using DEXseq, which revealed that tiRNA-Met

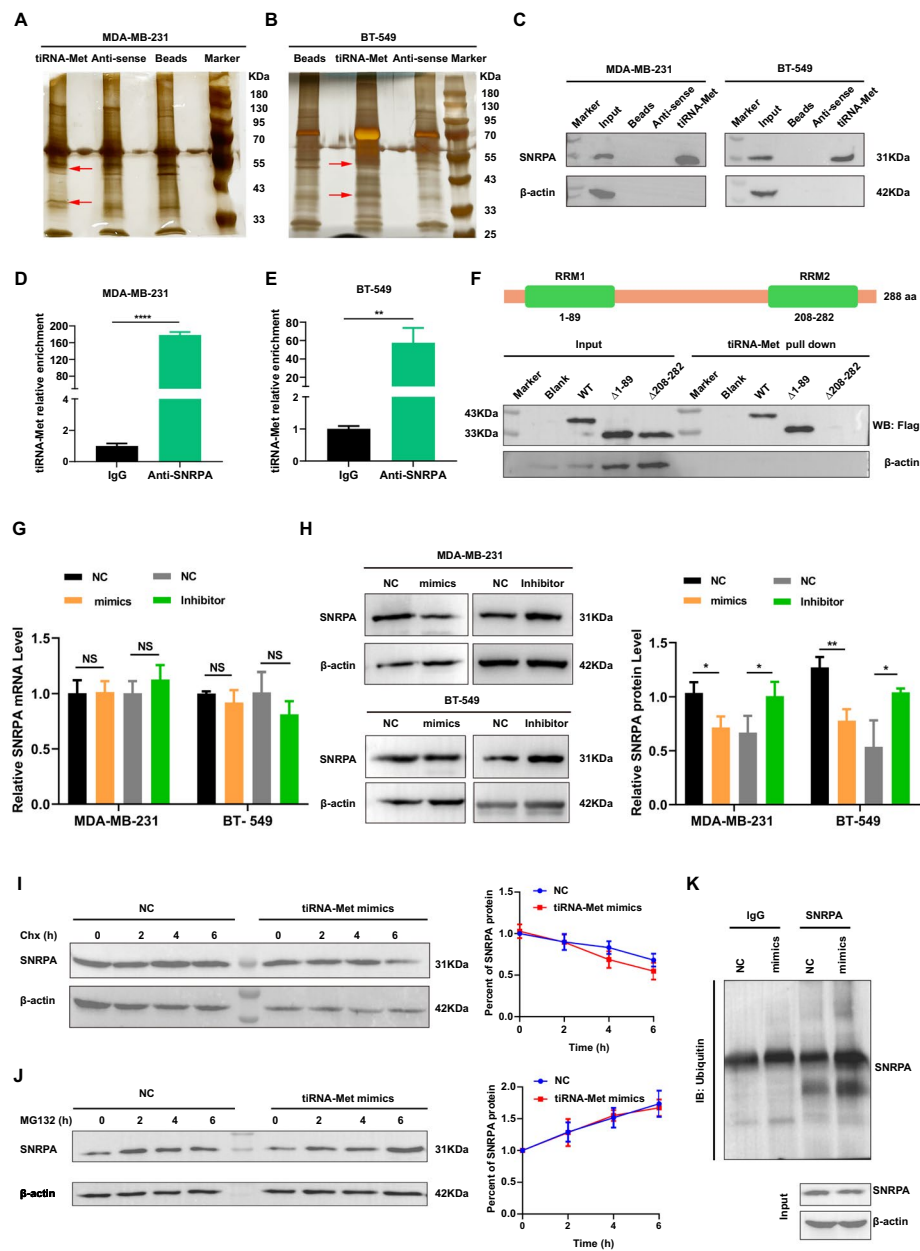


Fig. 2 tiRNA-Met directly interacted with SNRPA and promoted its ubiquitination. **A, B** Silver-stained SDS-PAGE gel images showed proteins immunoprecipitated by tiRNA-Met and its antisense RNA in MDA-MB-231 (**A**) and BT-549 (**B**) cell lines. **C** Western blot analysis of products from RNA pull-down assays using tiRNA-Met sense and antisense confirmed that tiRNA-Met directly associated with SNRPA. **D, E** RIP followed by RT-qPCR demonstrated specific binding of tiRNA-Met to SNRPA in MDA-MB-231 (**D**) and BT-549 (**E**) cells. **F** RNA pull-down and Western blot assays revealed that tiRNA-Met bound to the RRM2 domain of SNRPA. **G** The mRNA expression levels of *SNRPA* remained unchanged in MDA-MB-231 and BT-549 cells transfected with tiRNA-Met mimics or inhibitor. **H** Overexpression of tiRNA-Met reduced SNRPA protein levels in both cell lines, while inhibition of tiRNA-Met increased SNRPA protein levels. **I** MDA-MB-231 cells treated with cycloheximide (Chx; 5 μ M) and then transfected with tiRNA-Met mimics exhibited a reduced half-life of endogenous SNRPA protein, as shown by Western blot; β -actin served as a loading control. **J** Treatment with MG132 (20 μ g/ml) led to a progressive increase in SNRPA protein levels over time; β -actin was used as a reference. **K** Immunoprecipitation assays indicated that the binding of SNRPA to ubiquitinated proteins was elevated in MDA-MB-231 cells transfected with tiRNA-Met mimics. All data are presented as means \pm SD; ns, $P > 0.05$; * $P < 0.05$; ** $P < 0.01$; **** $P < 0.0001$

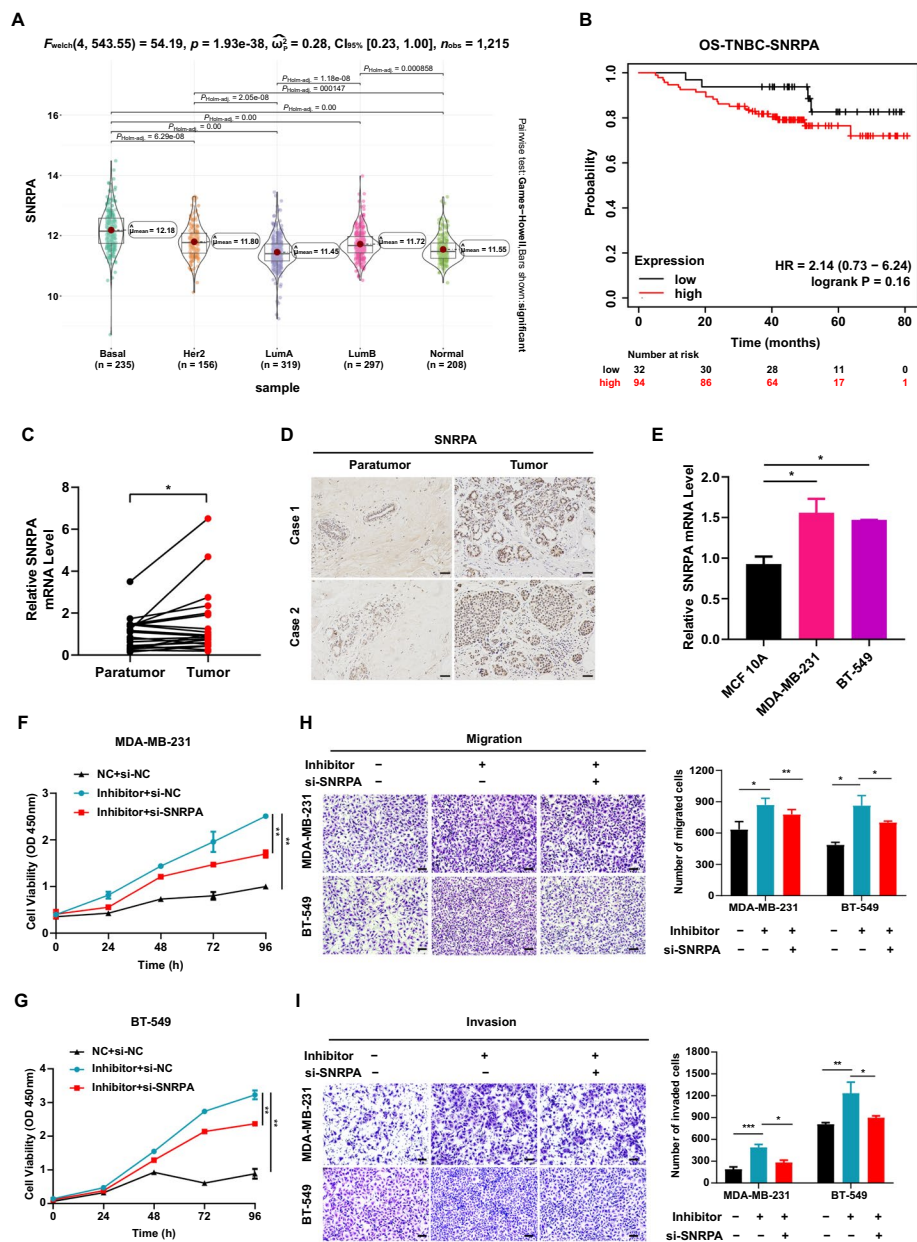


Fig. 3 Elevated SNRPA expression in TNBC tumor tissues and attenuation of SNRPA rescued the inhibitory effects of tiRNA-Met on TNBC cells. **A** Comparison of SNRPA expression levels revealed a significant elevation across different subtypes of breast cancer tissues, with the highest levels observed in basal-like breast cancer subtypes. **B** In a cohort of patients with TNBC ($n = 363$), higher SNRPA levels were negatively correlated with extended OS, although this correlation was not statistically significant ($P = 0.16$); log-rank test was utilized for statistical analysis. **C** RT-qPCR analysis revealed significantly increased *SNRPA* expression in TNBC tumor tissues compared with adjacent normal tissues ($n = 20$). **D** Immunohistochemistry results confirmed significant upregulation of SNRPA in TNBC tumor tissues. **E** *SNRPA* mRNA levels were elevated in MDA-MB-231 and BT-549 cell lines compared with MCF 10A. **F, G** Knockdown of SNRPA mitigated the tiRNA-Met inhibitor-induced cell proliferation in MDA-MB-231 (**F**) and BT-549 (**G**) cell lines. **H, I** SNRPA knockdown reversed the effects of the tiRNA-Met inhibitor on cell migration (**H**) and invasion (**I**) in both MDA-MB-231 and BT-549 cells. Scale bars represent 100 μm . All data are presented as means \pm SD; * $P < 0.05$; ** $P < 0.01$; *** $P < 0.001$

regulated the alternative splicing of 132 mRNAs, with 94 upregulated and 38 downregulated. However, *RANBP3L* was not among these differentially spliced genes (data not shown). An additional file provides this in more detail (see Additional file 1). We then examined whether SNRPA regulated *RANBP3L* expression by affecting its mRNA stability. Following treatment with the transcriptional inhibitor actinomycin D, transfection with si-SNRPA resulted in reduced degradation of endogenous *RANBP3L* mRNA in TNBC cells compared with the si-NC control (Fig. 4J, K). In addition, rescue assays demonstrated that suppression of tiRNA-Met led to decreased *RANBP3L* expression, which could be reversed by inhibiting SNRPA (Fig. 4L).

***RANBP3L* was downregulated in TNBC tissues and inhibited the proliferation and migration of TNBC cells**

RANBP3L, a member of the Ran binding protein family, has been relatively underexplored in tumor-related research [25]. To investigate its function, we conducted a bioinformatics analysis that revealed downregulation of *RANBP3L* across 21 different tumor types, including breast cancer (Supplementary Fig. S5A). Subsequently, we categorized the TCGA breast cancer dataset into distinct subtypes using PAM50 classification and observed that *RANBP3L* exhibited the lowest expression levels specifically in the basal-like breast cancer subtype (Fig. 5A). Furthermore, analysis with the UALCAN database confirmed that *RANBP3L* had the lowest expression levels in the TNBC subtype as well (Supplementary Fig. S5B). Moreover, *RANBP3L* expression was positively correlated with OS in both breast cancer (Supplementary Fig. S5C) and patients with TNBC (Fig. 5B). We further evaluated *RANBP3L* expression in human TNBC tissue samples, confirming that *RANBP3L* levels were significantly lower in tumor tissues than in adjacent normal tissues (Fig. 5C). Immunohistochemical analysis corroborated these findings, revealing a marked reduction in *RANBP3L* expression in human TNBC tissues compared with adjacent normal tissues (Fig. 5D). MDA-MB-231 and BT-549 cells also showed reduced *RANBP3L* expression compared with MCF10A cells (Fig. 5E). We next examined the effects of *RANBP3L* on TNBC cell phenotypes by increasing its level in TNBC cells (Supplementary Fig. S6A). The results indicated that increasing *RANBP3L* significantly repressed the proliferation (Fig. 5F–H), migration (Fig. 5I), and invasion (Fig. 5J) in both MDA-MB-231 and BT-549 cells.

tiRNA-Met inhibited the malignancy of TNBC cells via *RANBP3L*-mediated mTORC1/RPS6 signaling pathway

To further elucidate whether tiRNA-Met exerted its inhibitory effects on the malignant development of TNBC through its association with *RANBP3L*, we performed rescue experiments by transfecting tiRNA-Met mimics into cells with either *RANBP3L* knockdown or NC. The knockdown efficiency of *RANBP3L* was confirmed by RT-qPCR (Supplementary Fig. S6B, C). Knockdown of *RANBP3L* significantly diminished the inhibitory effects of tiRNA-Met on TNBC cell proliferation (Fig. 6A–C), migration (Fig. 6D, F), and invasion (Fig. 6E, G).

In addition, we conducted a correlation analysis between *RANBP3L* and all protein-coding genes in tumor datasets from the TCGA-BRCA cohort using the guilt-by-association method, assessing overlap with the Hallmark Collection. This analysis revealed

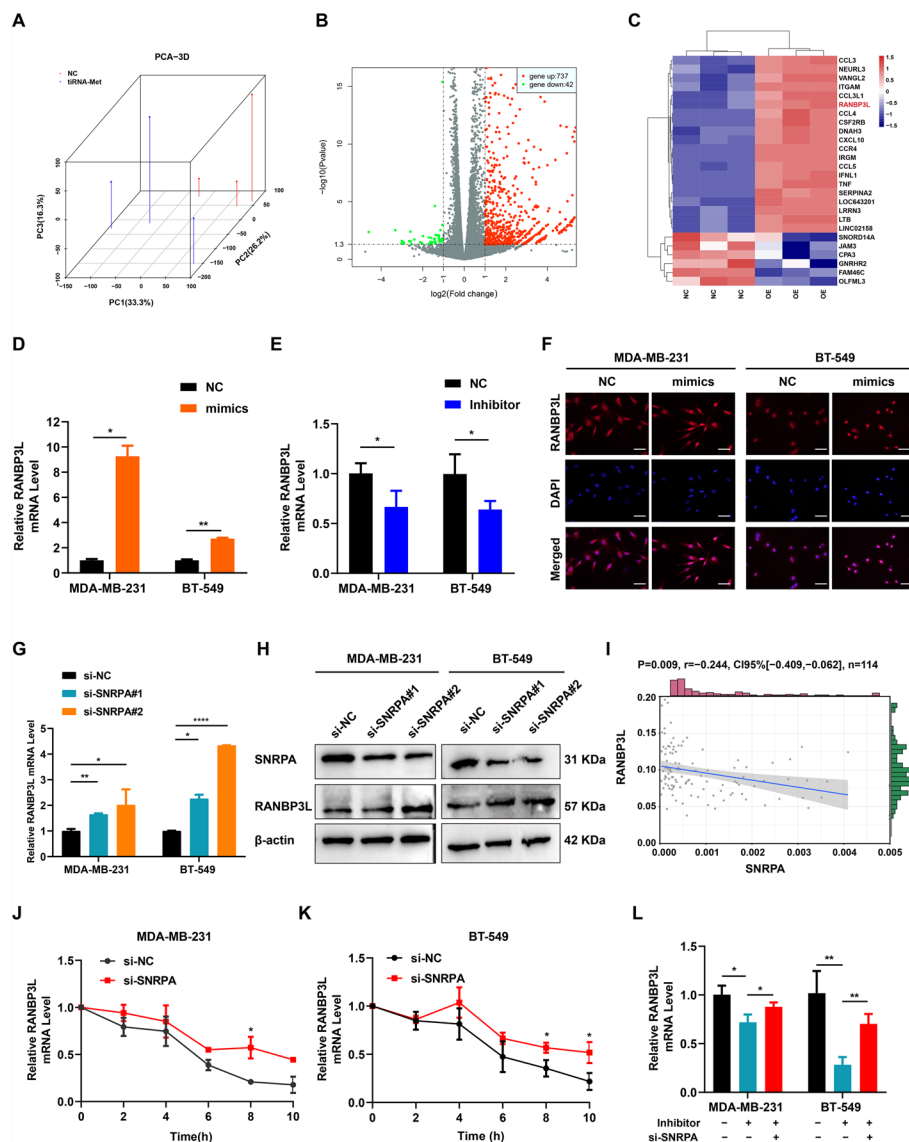


Fig. 4 tiRNA-Met upregulated the expression of *RANBP3L* via SNRPA. **A** Principal component analysis revealed distinct gene expression profiles between tiRNA-Met overexpressing cells and NC cells. **B** A volcano plot illustrated RNAs that were significantly differentially expressed (fold change > 2, $P < 0.05$). **C** RNA sequencing identified genes with differential expression between the two groups. **D** Overexpression of tiRNA-Met increased *RANBP3L* expression in MDA-MB-231 and BT-549 cell lines. **E** Inhibition of tiRNA-Met decreased *RANBP3L* expression in these cell lines. **F** Immunofluorescence assays confirmed that tiRNA-Met overexpression enhanced *RANBP3L* protein levels. **G** Inhibition of SNRPA resulted in increased mRNA levels of *RANBP3L* in both MDA-MB-231 and BT-549 cell lines. **H** SNRPA knockdown led to enhanced *RANBP3L* protein expression in MDA-MB-231 and BT-549 cells. **I** Correlation analysis of *RANBP3L* and SNRPA expression in TNBC samples from TCGA database. **J**, **K** SNRPA promoted degradation of *RANBP3L* mRNA in MDA-MB-231 (J) and BT-549 (K) cell lines, as shown by relative expression of *RANBP3L* mRNA in si-NC and si-SNRPA samples following actinomycin D treatment over 0–10 h. **L** RT-qPCR rescue experiments demonstrated that inhibition of tiRNA-Met, which downregulated *RANBP3L* expression, was reversed by SNRPA suppression. Scale bars represent 50 μ m. All data are presented as means \pm SD; * $P < 0.05$, ** $P < 0.01$, **** $P < 0.0001$

a link between *RANBP3L* and the mTORC1 signaling pathway (Fig. 6H). The phosphorylated form of ribosomal protein S6 (RPS6) acts as a surrogate marker for the activation of the mTORC1 pathway [26]. To explore the role of tiRNA-Met in regulating the

mTORC1/RPS6 pathway via RANBP3L, we co-transfected TNBC cells with a tiRNA-Met mimics and si-RANBP3L. The results showed that overexpression of tiRNA-Met did not alter the total protein levels of mTOR and RPS6. However, the expression of p-mTOR and p-RPS6 was significantly decreased. Notably, silencing RANBP3L partially restored p-mTOR and p-RPS6 levels in both TNBC cell lines (Fig. 6I, J). Collectively, these findings suggested that tiRNA-Met inhibited the mTORC1/RPS6 signaling pathway in TNBC cells by targeting RANBP3L, thereby suppressing the malignant progression of TNBC.

Upregulation of tiRNA-Met inhibited the growth of TNBC in vivo

To evaluate the therapeutic efficacy of tiRNA-Met overexpression in vivo, we generated stable lentiviral strains for a xenograft experiment (Fig. 7A). The tumor volume in the tiRNA-Met overexpression group was significantly smaller than that in the control group (Fig. 7B), and the average tumor weight was markedly reduced as well (Fig. 7C, D).

In addition, mRNA expression levels of tiRNA-Met and *RANBP3L* were significantly elevated in the xenograft tumor tissues of the tiRNA-Met overexpression group compared with the control group (Fig. 7E, F). Immunohistochemical analysis revealed that Ki-67 and SNRPA levels were decreased in the xenograft tumors of the tiRNA-Met overexpression group, while RANBP3L exhibited an opposite trend (Fig. 7G). Collectively, these findings highlighted tiRNA-Met overexpression as a promising therapeutic strategy to inhibit tumor growth in TNBC.

Discussion

Recent studies have revealed that tRFs, a novel class of noncoding RNAs, play significant roles in the development of various tumors. In the present study, we identified a unique human-specific tRNA half, tiRNA-Met, derived from mitochondrial tRNA^{Met-CAT}. This 29-nucleotide tiRNA-Met was predominantly localized in the cytoplasm and was significantly downregulated in TNBC tissues. Functionally, the upregulation of tiRNA-Met markedly inhibited the proliferation, migration, and invasion of TNBC cells, while its inhibition promoted malignancy. Our findings suggested that tiRNA-Met may function as an anti-tumorigenic tRF with potential as a diagnostic and prognostic marker, as well as a therapeutic target for TNBC.

Studies have shown that tRFs can modulate the malignant progression of tumors through various mechanisms. Similar to miRNAs, certain tRFs interacted directly with the 3'-UTR of target mRNAs, leading to translation inhibition [16, 27, 28]. Some tRFs orchestrate the entire translational machinery, acting as both suppressors and promoters. For instance, 5'-tiRNA^{Ala} and 5'-tiRNA^{Cys} inhibited the initiation of translation by partnering with the translational suppressor YB-1, which displaced the cap-binding complex eIF4G/A/F from capped mRNA, thereby facilitating the assembly of stress granules [29]. Furthermore, specific tRFs bound to proteins, altering their phosphorylation status, and consequently, their functional activity [14]. AS-tDR-007333 interacted with binding proteins to induce modifications in histones and activate transcription factors, thus enhancing promoter activity and resulting in changes in gene expression [19]. In addition, tiRNA-Gly bound directly to the UHM domain of the splicing-related RNA-binding protein RBM17, increasing its protein expression by inhibiting its ubiquitin/

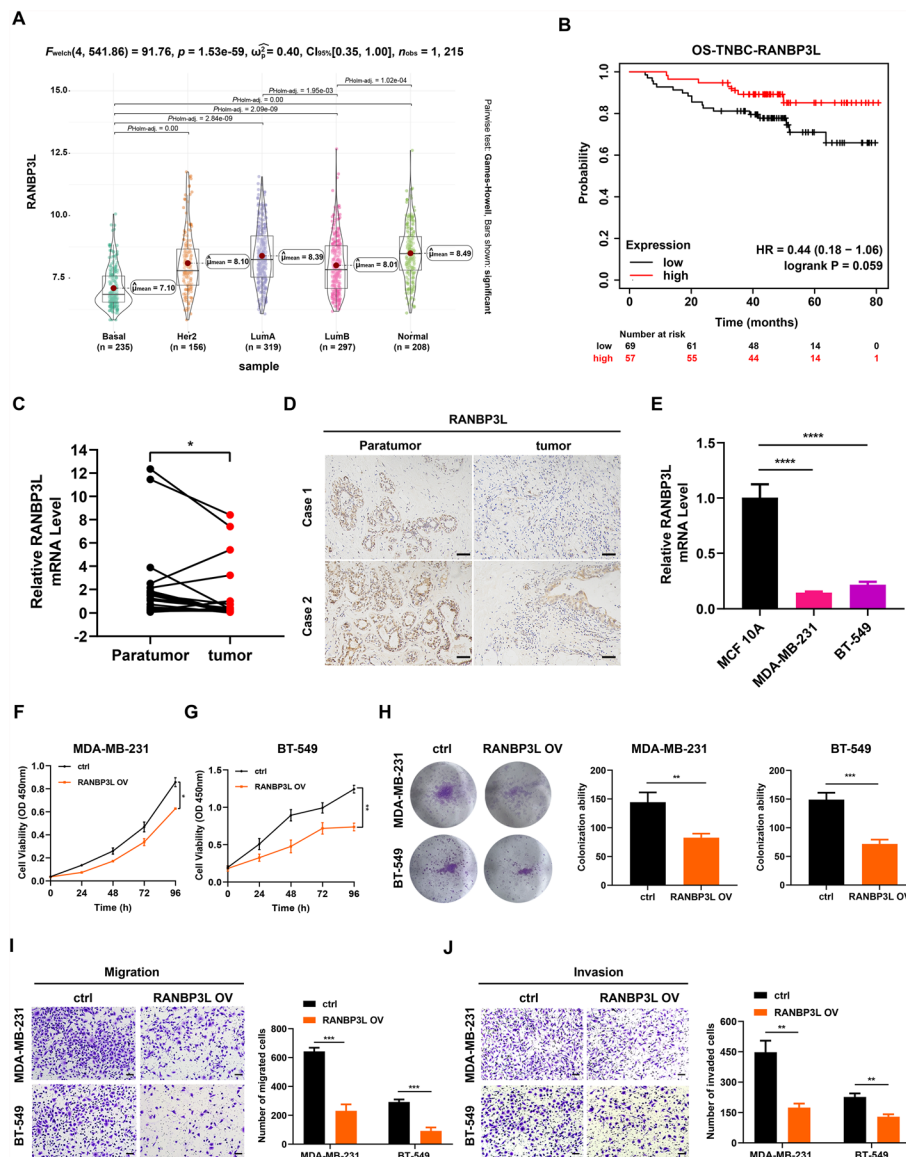


Fig. 5 RANBP3L was downregulated in TNBC tissues and inhibited the malignant progression of TNBC cells. **A** Comparison of RANBP3L expression levels showed a significant decrease in various subtypes of breast cancer tissues, with the lowest levels observed in basal-like breast cancer subtypes. **B** Kaplan–Meier analysis of patients with TNBC (n = 363) showed an association between lower RANBP3L levels and shorter OS (P = 0.059), analyzed using a log-rank test. **C** RT-qPCR confirmed significant downregulation of RANBP3L expression in TNBC tumor tissues compared with adjacent normal tissues (n = 20). **D** Immunohistochemistry results demonstrated significant downregulation of RANBP3L in TNBC tumor tissues. **E** RANBP3L mRNA levels were reduced in MDA-MB-231 and BT-549 cell lines compared with MCF 10A. **F–H** CCK-8 assays (**F**, **G**) and colony formation assays (**H**) showed that overexpression of RANBP3L reduced proliferation rates of MDA-MB-231 and BT-549 cells. **I**, **J** Transwell assays indicated that upregulation of RANBP3L decreased the number of migrated (**I**) and invaded (**J**) cells. Scale bars represent 50 μm. All data are presented as means ± SD; *P < 0.05, **P < 0.01, ***P < 0.001, ****P < 0.0001

proteasome-dependent degradation [17]. In the present study, we demonstrated that tRNA-Met directly bound to the RRM2 domain of RNA-binding protein SNRPA. SNRPA is composed of 282 encoded amino acids and functions as a component of the

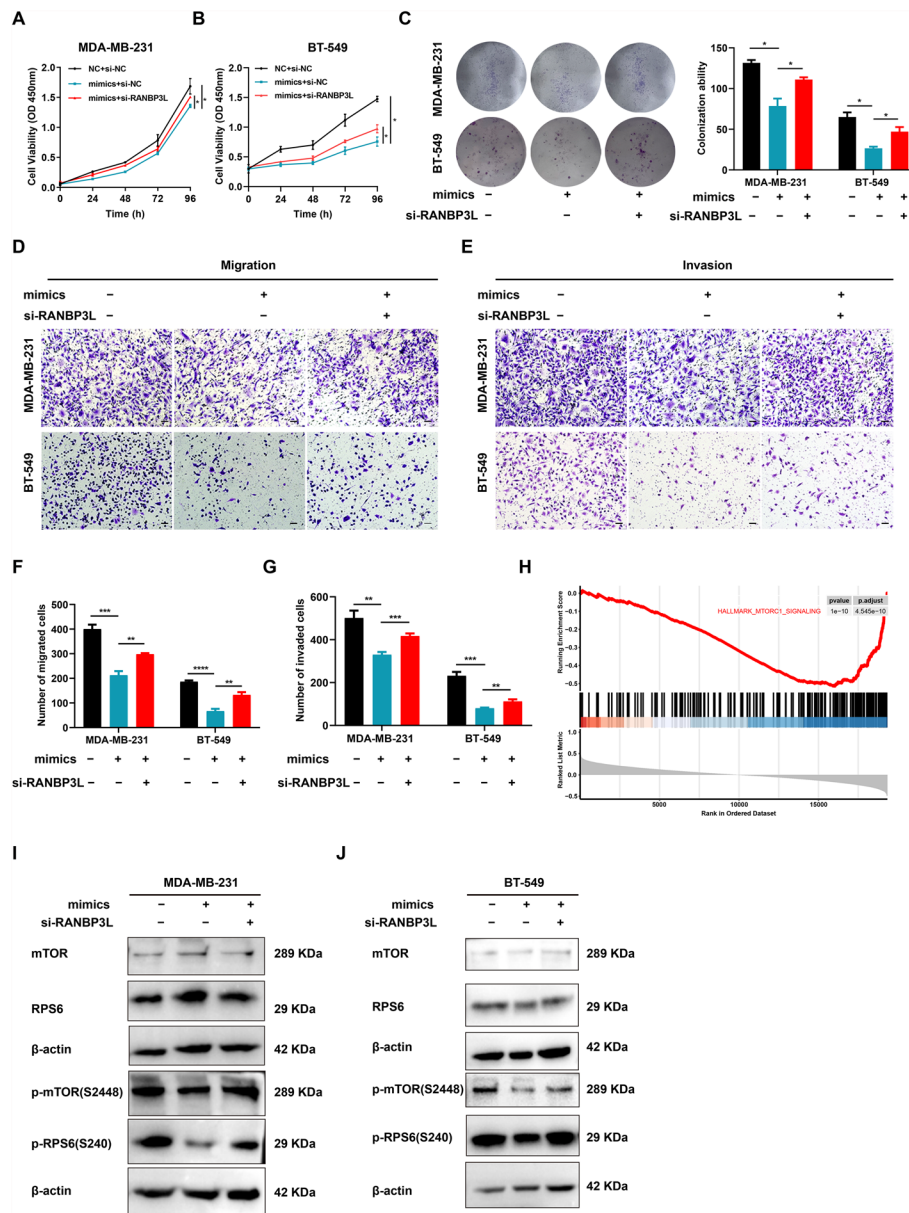


Fig. 6 tiRNA-Met inhibited the malignancy of TNBC cells via a RANBP3L-mediated mTORC1/RPS6 signaling pathway. **A, B** Rescue experiments showed that RANBP3L knockdown partially abrogated the effects of tiRNA-Met overexpression on cell proliferation rates in MDA-MB-231 (**A**) and BT-549 (**B**) cells. **C** RANBP3L knockdown partially reduced the impact of tiRNA-Met overexpression on colony formation. **D–G** The inhibitory effects of tiRNA-Met on cell migration (**D, F**) and invasion (**E, G**) were reversed by RANBP3L suppression. **H** Guilt-by-association analysis linked RANBP3L to the mTORC1 signaling pathway. **I, J** Western blot analysis indicated that tiRNA-Met overexpression significantly reduced p-mTOR and p-RPS6 expression levels, which were partially restored by silencing RANBP3L in MDA-MB-231 (**I**) and BT-549 (**J**) cell lines. Scale bars represent 50 μ m. All data are presented as means \pm SD; * P < 0.05, ** P < 0.01, *** P < 0.001, **** P < 0.0001

U1 small nuclear ribonucleoprotein (U1 snRNP) complex, which is critical for mRNA polyadenylation, spliceosome assembly, and splicing [24, 30, 31]. Previous studies have indicated that SNRPA was highly expressed in various human cancers. SNRPA promotes the malignant progression of gastric cancer by regulating the expression of nerve

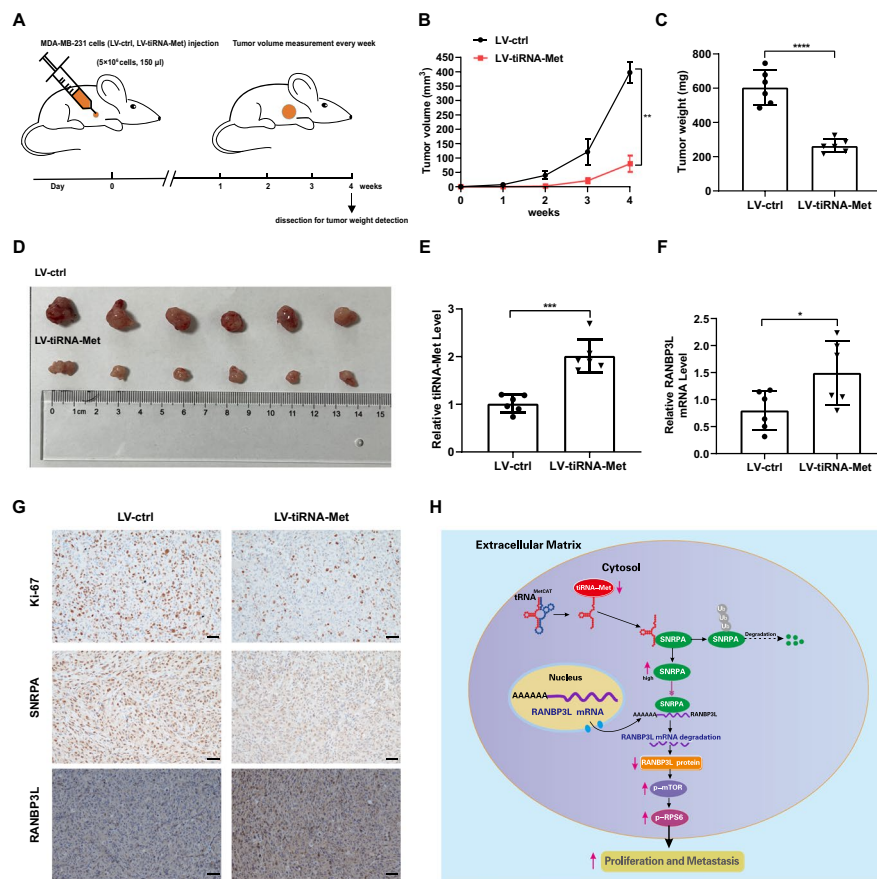


Fig. 7 Overexpression of tiRNA-Met diminished TNBC tumor growth in vivo. **A** Schematic representation of the subcutaneous tumorigenesis procedure. **B** The LV-tiRNA-Met group exhibited a significantly smaller average tumor volume compared with the LV-ctrl group. **C** Average tumor weight was significantly lower in the LV-tiRNA-Met group than in the LV-ctrl group. **D** Representative images of xenograft tumors isolated from the LV-ctrl and LV-tiRNA-Met groups (n = 6). **E**, **F** RT-qPCR analysis revealed that tiRNA-Met overexpression increased expression levels of tiRNA-Met (**E**) and RANBP3L (**F**) in xenograft tumor tissues (n = 6). **G** Immunohistochemistry staining images demonstrated that tiRNA-Met overexpression resulted in decreased expression levels of Ki-67 and SNRPA, alongside increased expression of RANBP3L in xenograft tumors. Scale bars represent 50 µm. **H** A schematic illustration delineating the mechanism by which tiRNA-Met impeded tumorigenesis in TNBC via the SNRPA-RANBP3L pathway. All data are presented as mean ± SD; *P < 0.05, **P < 0.01, ***P < 0.001, ****P < 0.0001

growth factor [23]. It has also been shown to be overexpressed in lung adenocarcinoma and squamous cell carcinoma tissues, where its levels negatively correlated with patient prognosis [32]. Moreover, SNRPA facilitated metastasis in hepatocellular carcinoma via activation of the Notch1/Snail signaling pathway [33]. Bioinformatics analyses in our study revealed that SNRPA was highly expressed in all four subtypes of breast cancer, with the highest levels observed in TNBC. Notably, this expression was negatively correlated with patient survival. Our data further demonstrated that SNRPA was markedly elevated in TNBC tissues and cell lines. We found that interaction with tiRNA-Met led to a marked reduction in SNRPA protein expression, as tiRNA-Met promoted its degradation via ubiquitin/proteasome-dependent pathways. Rescue assays indicated that the effects of tiRNA-Met on cell proliferation, migration, and invasion were reversed by

SNRPA. These results revealed a novel mechanism by which tRF interacted with SNRPA to regulate the malignancy of TNBC cells.

To elucidate how tiRNA-Met regulated downstream target genes through SNRPA, we analyzed the transcriptome changes induced by tiRNA-Met and identified RANBP3L as a key target gene. Notably, tiRNA-Met upregulated RANBP3L expression, while SNRPA negatively regulated it. The regulatory mechanisms controlling RANBP3L expression are largely unexplored. To determine whether tiRNA-Met can mediate the alternative splicing of RANBP3L through its interaction with SNRPA, we used DEXseq to analyze the RNA sequencing results from the tiRNA-Met overexpression model and found that tiRNA-Met regulated the alternative splicing of 132 mRNAs; however, RANBP3L was not among these differentially spliced genes. Subsequently, we aimed to verify whether SNRPA affected RANBP3L stability. We found that SNRPA regulated RANBP3L expression by influencing its mRNA stability, as evidenced by reduced degradation of endogenous *RANBP3L* mRNA in TNBC cells following si-SNRPA transfection. In addition, suppression of tiRNA-Met decreased RANBP3L expression, an effect that could be reversed by inhibiting SNRPA. These findings underscored the important role of SNRPA in regulating RANBP3L stability during the regulation of tiRNA-Met.

The *RANBP3L* gene, located on chromosome 5, encodes a protein that contains a highly conserved Ran-binding domain (RBD) in its structure. Ran, a small GTPase of the Ras superfamily, is essential for nucleocytoplasmic transport and cell cycle progression [34]. RANBP3L specifically mediates the nuclear export of Smad1/5/8 proteins, which are essential effectors in bone morphogenetic protein (BMP) signaling, and it also contributes to BMP-mediated differentiation of mesenchymal stem cells [35]. To date, only a few studies have been published regarding the role of RANBP3L in tumors. In renal cell carcinoma, the loss of RANBP3L led to the acquisition of a clear cell carcinoma-like phenotype by renal epithelial cells [25]. High-salt treatment resulted in a significant upregulation of tumor suppressor genes, including RANBP3L, in breast cancer cells [36]. In the present study, bioinformatics analysis revealed that RANBP3L was expressed at low levels in all four subtypes of breast cancer, with the lowest expression observed in TNBC. Notably, its expression was positively correlated with patient survival. Furthermore, our experimental data confirmed that RANBP3L exhibited low expression in TNBC tissues and cell lines. Overexpression of RANBP3L inhibited the proliferation, migration, and invasion of TNBC cells, functions similar to those of tiRNA-Met. Rescue assays showed that the inhibitory effect of tiRNA-Met overexpression on the malignant progression of TNBC cells can be reversed by RANBP3L suppression. Collectively, these findings indicated that tiRNA-Met enhanced the expression of RANBP3L, which subsequently acted as a tumor suppressor to inhibit the malignancy of TNBC. Through gene set enrichment analysis, we identified that RANBP3L was associated with the mTORC1 signaling pathway. RPS6, a crucial component of the 40S ribosomal subunit, exists in a phosphorylated form (p-RPS6) that serves as a reliable marker for the activation of the mTORC1 pathway, which is implicated in numerous cancer types. The activation of the mTORC1/RPS6 pathway was associated with cancer cell survival and was regulated by various upstream factors [26, 37]. Phosphorylation of RPS6 reduced DNA damage induced by Kras and diminished p53-mediated tumor suppression in pancreatic cancer [38]. Elevated levels of p-RPS6 at Ser240 correlated with increased Ki67 expression and

shorter OS in patients with breast cancer [37]. Our experimental results showed that while the overexpression of tiRNA-Met did not significantly alter the total protein levels of mTOR and RPS6, the expressions of p-mTOR and p-RPS6 were markedly decreased, an effect that could be reversed by inhibiting RANBP3L. These findings suggested a critical role for the tiRNA-Met–RANBP3L interaction in modulating the mTORC1 signaling pathway.

Conclusions

In summary, our study revealed that tiRNA-Met, a human-specific tRF derived from mitochondrial tRNA^{Met-CAT}, served as a critical tumor suppressor in TNBC. The significant downregulation of tiRNA-Met in TNBC tissues was associated with enhanced tumorigenic characteristics, including increased cell proliferation, migration, and invasion. Mechanistically, tiRNA-Met mediated its antitumor effects through interaction with the RNA-binding protein SNRPA, facilitating its ubiquitination and degradation. This process stabilized *RANBP3L* mRNA, leading to the inhibition of phosphorylation of key components in the mTORC1 signaling pathway (Fig. 7H). These findings underscored the potential of tiRNA-Met as a novel diagnostic and prognostic biomarker and position it as a promising therapeutic target for TNBC, warranting further exploration of its clinical applications.

Abbreviations

AR	Androgen receptor
BMP	Bone morphogenetic protein
circRNAs	Circular RNAs
EGFR	Epidermal growth factor receptor
ER	Estrogen receptors
HER2	Human epidermal growth factor receptor 2
HNRNPL	Heterogeneous nuclear ribonucleoprotein L
lncRNAs	Long noncoding RNAs
miRNAs	MicroRNAs
ncRNAs	Noncoding RNAs
OS	Overall survival
PARP	Poly (ADP-ribose) polymerase
PR	Progesterone receptors
RANBP3L	Ran-binding protein 3-like
RBD	Ran-binding domain
RRM2	RNA recognition motif 2
sncRNAs	Small noncoding RNAs
SD	Standard deviation
SNRPA	Small nuclear ribonucleoprotein A
TNBC	Triple-negative breast cancer
U1 snRNP	U1 small nuclear ribonucleoprotein
tRFs	tRNA-derived fragments
UTR	Untranslated region
VEGF	Vascular endothelial growth factor

Supplementary Information

The online version contains supplementary material available at <https://doi.org/10.1186/s11658-025-00738-2>.

Additional file 1: tiRNA-Met Overexpression Altered Alternative Splicing Events in MDA-MB-231 Cells. This file contained relevant figure showing the effects of tiRNA-Met overexpression on alternative splicing events in MDA-MB-231 cells.

Additional file 2.

Additional file 3.

Additional file 4.

Acknowledgements

Funded by the Natural Science Foundation of Shanghai, the National Natural Science Foundation of China, and the China Postdoctoral Science Foundation.

Author contributions

L.J.J. and S.Y.B. were responsible for the experimental design and conducted the majority of the experiments. Z.X.F. and Z.P. contributed to conducting specific portions of the experiments. Z.L.Z. conducted the collection of specimens. X.B.J. contributed to data analysis. W.X. was responsible for pathological associated data analysis. Z.W. and Z.P. provided financial support and guidance for the project.

Funding

This work was supported by the National Natural Science Foundation of China (82173309, 81874121), the Natural Science Foundation of Shanghai (21ZR1409700), and China Postdoctoral Science Foundation (2024M751534).

Availability of data and materials

The datasets generated in this study are available from the corresponding author upon reasonable request.

Declarations

Ethics approval and consent to participate

The study was conducted with the approval of the Ethics Committee of the School of Basic Medical Sciences, Fudan University (approval no. 2021-C025; date: 10/15/2021). All participants provided written informed consent, and the project was carried out in accordance with the guidelines set forth in both the Declaration of Helsinki and the Basel Declaration. All animal experiments received approval from the Ethics Committee for Laboratory Animals of the School of Basic Medical Sciences, Fudan University (approval no. 20210302-001; date: 03/02/2021). In compliance with the committee's stipulation that the maximum diameter of tumors must not exceed 15 mm, this study ensured that all tumors remained below this threshold. Furthermore, all animal research was conducted in accordance with the Basel Declaration and the National Research Council's Guidelines for the Care and Use of Laboratory Animals.

Consent for publication

Not applicable.

Competing interests

The authors declare no competing interests.

Received: 15 December 2024 Accepted: 25 April 2025

Published online: 23 May 2025

References

1. Sung H, Ferlay J, Siegel RL, Laversanne M, Soerjomataram I, Jemal A, et al. Global cancer statistics 2020: GLOBOCAN estimates of incidence and mortality worldwide for 36 cancers in 185 countries. *CA Cancer J Clin*. 2021;71(3):209–49.
2. da Silva JL, Cardoso Nunes NC, Izetti P, de Mesquita GG, de Melo AC. Triple negative breast cancer: a thorough review of biomarkers. *Crit Rev Oncol Hematol*. 2020;145:102855.
3. Derakhshan F, Reis-Filho JS. Pathogenesis of triple-negative breast cancer. *Annu Rev Pathol*. 2022;17:181–204.
4. Dong S, Yousefi H, Savage IV, Okpechi SC, Wright MK, Matossian MD, et al. Ceritinib is a novel triple negative breast cancer therapeutic agent. *Mol Cancer*. 2022;21(1):138.
5. Jain V, Kumar H, Anod HV, Chand P, Gupta NV, Dey S, et al. A review of nanotechnology-based approaches for breast cancer and triple-negative breast cancer. *J Control Release*. 2020;326:628–47.
6. Mo W, Liu Q, Lin CC, Dai H, Peng Y, Liang Y, et al. mTOR inhibitors suppress homologous recombination repair and synergize with PARP inhibitors via regulating suv39h1 in BRCA-proficient triple-negative breast cancer. *Clin Cancer Res*. 2016;22(7):1699–712.
7. Slack FJ, Chinnaiyan AM. The role of non-coding RNAs in oncology. *Cell*. 2019;179(5):1033–55.
8. Wu P, Mo Y, Peng M, Tang T, Zhong Y, Deng X, et al. Emerging role of tumor-related functional peptides encoded by lncRNA and circRNA. *Mol Cancer*. 2020;19(1):22.
9. Fu M, Gu J, Wang M, Zhang J, Chen Y, Jiang P, et al. Emerging roles of tRNA-derived fragments in cancer. *Mol Cancer*. 2023;22(1):30.
10. Goodarzi H, Liu X, Nguyen HC, Zhang S, Fish L, Tavazoie SF. Endogenous tRNA-derived fragments suppress breast cancer progression via YBX1 displacement. *Cell*. 2015;161(4):790–802.
11. Kim HK, Fuchs G, Wang S, Wei W, Zhang Y, Park H, et al. A transfer-RNA-derived small RNA regulates ribosome biogenesis. *Nature*. 2017;552(7683):57–62.
12. Schaffer AE, Eggens VR, Caglayan AO, Reuter MS, Scott E, Coufal NG, et al. CLP1 founder mutation links tRNA splicing and maturation to cerebellar development and neurodegeneration. *Cell*. 2014;157(3):651–63.

13. Zhu L, Ge J, Li T, Shen Y, Guo J. tRNA-derived fragments and tRNA halves: the new players in cancers. *Cancer Lett.* 2019;452:31–7.
14. Pan L, Huang X, Liu ZX, Ye Y, Li R, Zhang J, et al. Inflammatory cytokine-regulated tRNA-derived fragment tRF-21 suppresses pancreatic ductal adenocarcinoma progression. *J Clin Invest.* 2021;131:22.
15. Yu M, Yi J, Qiu Q, Yao D, Li J, Yang J, et al. Pan-cancer tRNA-derived fragment CAT1 coordinates RBPMS to stabilize NOTCH2 mRNA to promote tumorigenesis. *Cell Rep.* 2023;42(11): 113408.
16. Mo D, Jiang P, Yang Y, Mao X, Tan X, Tang X, et al. A tRNA fragment, 5'-tRNA(Val), suppresses the Wnt/beta-catenin signaling pathway by targeting FZD3 in breast cancer. *Cancer Lett.* 2019;457:60–73.
17. Han L, Lai H, Yang Y, Hu J, Li Z, Ma B, et al. A 5'-tRNA halve, tRNA-Gly promotes cell proliferation and migration via binding to RBM17 and inducing alternative splicing in papillary thyroid cancer. *J Exp Clin Cancer Res.* 2021;40(1):222.
18. Cui H, Li H, Wu H, Du F, Xie X, Zeng S, et al. A novel 3' tRNA-derived fragment tRF-Val promotes proliferation and inhibits apoptosis by targeting EEF1A1 in gastric cancer. *Cell Death Dis.* 2022;13(5):471.
19. Yang W, Gao K, Qian Y, Huang Y, Xiang Q, Chen C, et al. A novel tRNA-derived fragment AS-tDR-007333 promotes the malignancy of NSCLC via the HSPB1/MED29 and ELK4/MED29 axes. *J Hematol Oncol.* 2022;15(1):53.
20. Lu S, Wei X, Tao L, Dong D, Hu W, Zhang Q, et al. A novel tRNA-derived fragment tRF-3022b modulates cell apoptosis and M2 macrophage polarization via binding to cytokines in colorectal cancer. *J Hematol Oncol.* 2022;15(1):176.
21. Zhu P, Lu J, Zhi X, Zhou Y, Wang X, Wang C, et al. tRNA-derived fragment tRFLys-CTT-010 promotes triple-negative breast cancer progression by regulating glucose metabolism via G6PC. *Carcinogenesis.* 2021;42(9):1196–207.
22. Bhatia S, Kramer M, Russo S, Naik P, Arun G, Brophy K, et al. Patient-derived triple-negative breast cancer organoids provide robust model systems that recapitulate tumor intrinsic characteristics. *Cancer Res.* 2022;82(7):1174–92.
23. Dou N, Yang D, Yu S, Wu B, Gao Y, Li Y. SNRPA enhances tumour cell growth in gastric cancer through modulating NGF expression. *Cell Prolif.* 2018;51(5): e12484.
24. Qiu F, Fu Y, Lu C, Feng Y, Wang Q, Huo Z, et al. Small nuclear ribonucleoprotein polypeptide a-mediated alternative polyadenylation of STAT5B during Th1 cell differentiation. *J Immunol.* 2017;199(9):3106–15.
25. Chernyakov D, Gross A, Fischer A, Bornkessel N, Schultheiss C, Gerloff D, et al. Loss of RANBP3L leads to transformation of renal epithelial cells towards a renal clear cell carcinoma like phenotype. *J Exp Clin Cancer Res.* 2021;40(1):226.
26. Gambardella V, Gimeno-Valiente F, Tarazona N, Martinez-Ciarpaglini C, Roda D, Fleitas T, et al. NRF2 through RPS6 activation is related to anti-HER2 drug resistance in HER2-amplified gastric cancer. *Clin Cancer Res.* 2019;25(5):1639–49.
27. Huang B, Yang H, Cheng X, Wang D, Fu S, Shen W, et al. tRF/miR-1280 suppresses stem cell-like cells and metastasis in colorectal cancer. *Cancer Res.* 2017;77(12):3194–206.
28. Jiang Q, Ma Y, Zhao Y, Yao MD, Zhu Y, Zhang QY, et al. tRNA-derived fragment tRF-1001: a novel anti-angiogenic factor in pathological ocular angiogenesis. *Mol Ther Nucleic Acids.* 2022;30:407–20.
29. Ivanov P, Emara MM, Villen J, Gygi SP, Anderson P. Angiogenin-induced tRNA fragments inhibit translation initiation. *Mol Cell.* 2011;43(4):613–23.
30. Subramania S, Gagne LM, Campagne S, Fort V, O'Sullivan J, Mocaer K, et al. SAM68 interaction with U1A modulates U1 snRNP recruitment and regulates mTor pre-mRNA splicing. *Nucleic Acids Res.* 2019;47(8):4181–97.
31. Zhang Y, Wang X, Wang H, Jiang Y, Xu Z, Luo L. Elevated small nuclear ribonucleoprotein polypeptide an expression correlated with poor prognosis and immune infiltrates in patients with hepatocellular carcinoma. *Front Oncol.* 2022;12:893107.
32. Yuan M, Yu C, Chen X, Wu Y. Investigation on potential correlation between small nuclear ribonucleoprotein polypeptide A and lung cancer. *Front Genet.* 2020;11:610704.
33. Mo Z, Li R, Cao C, Li Y, Zheng S, Wu R, et al. Splicing factor SNRPA associated with microvascular invasion promotes hepatocellular carcinoma metastasis through activating NOTCH1/Snail pathway and is mediated by circSEC62/miR-625–5p axis. *Environ Toxicol.* 2023. <https://doi.org/10.1002/tox.23745>.
34. Boudhraa Z, Carmona E, Provencher D, Mes-Masson AM. Ran GTPase: a key player in tumor progression and metastasis. *Front Cell Dev Biol.* 2020;8:345.
35. Chen F, Lin X, Xu P, Zhang Z, Chen Y, Wang C, et al. Nuclear export of Smads by RanBP3L regulates bone morphogenetic protein signaling and mesenchymal stem cell differentiation. *Mol Cell Biol.* 2015;35(10):1700–11.
36. Sharma M, Dey U, Das AS, Olymon K, Kumar A, Mukhopadhyay R. Anti-tumor potential of high salt in breast cancer cell lines. *Mol Biol Rep.* 2024;51(1):1002.
37. Yi YW, You KS, Park JS, Lee SG, Seong YS. Ribosomal protein S6: a potential therapeutic target against cancer? *Int J Mol Sci.* 2021;23(1):48.
38. Khalailah A, Dreazen A, Khatib A, Apel R, Swisa A, Kidess-Bassir N, et al. Phosphorylation of ribosomal protein S6 attenuates DNA damage and tumor suppression during development of pancreatic cancer. *Cancer Res.* 2013;73(6):1811–20.

Publisher's Note

Springer Nature remains neutral with regard to jurisdictional claims in published maps and institutional affiliations.